

Electrolyte Chemistry Towards Improved Cycling Stability in Na-Based Dual-Ion Batteries with High-Power/Energy Storage

Xian-Kun Hou⁺,^[a] Shao-Fang Li⁺,^[a] Wen-Hao Li,^[b] Hao-Jie Liang,^[b] Zhen-Yi Gu,^[b] Xiao-Xi Luo,^[a] and Xing-Long Wu^{*[a, b]}

Dual-ion batteries (DIBs) have attracted great research interests owing to the co-utilization of cation and anion as charge carriers. Unlike the low energy density (E_{den}) of supercapacitors and halogen-ion batteries also with anion working, graphite-cathode-based DIBs exhibit obviously higher E_{den} with high working voltage. However, general electrolytes cannot satisfy the high-energy demand for Na-based DIBs with high power density. Herein, we design an effective electrolyte with optimized performance to limit the occurrence of side reactions during cycling, improving the cycling stability and E_{den} of Na-based DIBs. Such electrolyte-modified Na-DIBs exhibit higher

discharge plateau and specific capacity compared to the pristine batteries, contribute preeminent E_{den} of 370.4 Wh/kg at a high-power density of 8888.4 W/kg (2.0 A/g), and deliver higher capacity retention of 72% after 1000 cycles under 40 °C (1.0 A/g). All of these improvements are attributed to the interphase protection of anode/cathode by modified electrolyte, and the increase of diffusion ability under high potential. This strategy not only provides reference significance for enhancing the performance of DIBs, but also promotes the development of DIBs with high-power/energy and long-term cycle working condition.

1. Introduction

In the 1990s, soon after the commercial application of lithium-ion batteries (LIBs), Carlin and coworkers reported advanced dual-ion batteries (DIBs) in which graphite was used as both anode and cathode.^[1] In contrast to the “rocking chair” single-cation batteries, such as LIBs and sodium-ion batteries (SIBs),^[2] DIBs employ both cation and anion to store electric energy. In fact, energy-storage contribution of DIBs is mainly determined by the number and type of anions (such as PF_6^- , AlCl_4^- , TFSI^- , BF_4^- , FSI^- , etc.)^[3] in the graphite intercalation compounds (GICs).^[4] Actually, there are also other anion-based electrochemical energy-storage (EES) devices including supercapacitors (SCs)^[5] and halogen-ion batteries (HIBs, such as fluoride-ion batteries).^[6] By comparison, DIBs show much higher energy density due to the double-electrode de-/intercalation reactions, lower manufacturing cost and higher safety than SCs and HIBs, suggesting the wider application possibility and range of DIBs.

In order to meet the low-cost design concept of DIBs, Na-based DIBs (Na-DIBs) have developed rapidly because of the cheaper price of Na than other elements, such as Li in Li-based

DIBs. Na-DIBs are expected to be suitable for large-scale storage devices in the future.^[7] However, although the discharge (working) plateau of Na-DIBs is higher than 4.5 V,^[8] the storage capacity is limited in anion-based GICs. Hence, the energy density of general Na-DIBs still cannot surpass the mature commercial LIBs. Besides, due to the larger ionic size of Na ions and lower Lewis acidity,^[3b,9] electrochemical performance of Na-DIBs in general electrolyte is extremely unstable under high-power condition, resulting in the harmful diving phenomenon during cycling, *viz.*, a sudden decrease of specific capacity, Coulombic efficiency and/or output voltage during cycling.^[10] Such a diving phenomenon implies the serious damage of cycling stability of batteries. Obviously, poor cycling performance with diving phenomenon cannot support the practical development of DIBs. Fortunately, in contrast to the “rocking chair” single-cation batteries, electrolytes have the more important contribution to improve the performance of DIBs,^[3b] and novel electrolyte design is of profound significance for DIBs. However, most of previous studies focus on Li-DIBs,^[11] and less on Na-DIBs.^[3d,12]

Herein, we have studied a novel electrolyte which contains 3 mol L⁻¹ NaPF_6 in ethylene carbonate (EC):ethyl methyl carbonate (EMC)=1:1 with 10% fluoroethylene carbonate (FEC), thereafter abbreviated as 3 MF, and enhanced the comprehensive energy-storage performance of Na-DIBs including the avoidance of diving phenomenon. As a result, the Na-DIBs in 3 MF exhibit outstanding cycling stability and high E_{den} without the presence of diving phenomenon. For example, 3 MF DIBs contribute superhigh E_{den} of 424.27 Wh/kg (based on active materials) compared to SCs and HIBs. Even at a large current density of 2.0 A/g, its E_{den} value still remains at 370.35 Wh/kg with an ultrahigh power density of 8888.4 W/kg.

[a] X.-K. Hou,⁺ S.-F. Li,⁺ X.-X. Luo, Prof. X.-L. Wu
Faculty of Chemistry
Northeast Normal University
Changchun, Jilin 130024, P. R. China
E-mail: xinglong@nenu.edu.cn

[b] W.-H. Li, H.-J. Liang, Z.-Y. Gu, Prof. X.-L. Wu
MOE Key Laboratory for UV Light-Emitting Materials and Technology
Northeast Normal University
Changchun, Jilin 130024, P. R. China

[†]The authors contributed equally to this work.

Supporting information for this article is available on the WWW under
<https://doi.org/10.1002/batt.202100124>

Under 40 °C, the 3 MF DIBs also exhibit high capacity retention of 72% after 1000 cycles at 1.0 A/g. Moreover, the influences of electrolyte on anode and cathode interphase are ascertained by powder X-ray diffraction (XRD), scanning electron microscope (SEM) and X-ray photoelectron spectroscopy (XPS) analyses. It is realized that 3 MF electrolyte decreases the polarization of Na anode during deposition/stripping and increases the structure stability of graphite cathode, resulting in the final improvement of battery performance.

2. Results and Discussion

In addition to the optimized 3 MF electrolyte, other three electrolytes, i.e., 0.5 mol L⁻¹ NaPF₆ in EC:EMC=1:1 with 10% FEC (0.5 MF), 0.5 mol L⁻¹ NaPF₆ in EC:EMC=1:1 (0.5 M), and 3 mol L⁻¹ NaPF₆ in EC:EMC=1:1 (3 M), were also explored to compare the electrochemical properties of Na-DIBs with graphite cathode. As shown in Figure S1a, esters of EC and EMC are used as the main solvents because of their workability at high voltage in NaPF₆-based DIBs, higher capacity than other ester solvents.^[8b,13] Moreover, the explorations and discussions of different concentrations and different FEC usage are also presented in the Figure S1b c. Figure 1a are the linear sweep voltammetry (LSV) curves of four electrolytes (0.5 M, 0.5 MF, 3 M and 3 MF) measured at 2 mV/s. Compared with 0.5 M electrolyte, Na-DIBs with 0.5 MF shows an obvious anodic peak started at about 4.05 V, implying the decomposition of FEC and the decrease of initial electrochemical window of electrolyte after FEC addition. This behavior is harmful to the high-potential working of DIBs. In general, higher salt-content electrolytes have wider electrochemical window,^[14] and the property of 3 M and 3 MF is consistent with previous researches. Unlike 3 M electrolyte, a tiny anodic peak appears

in 3 MF curves at 3.9 V, which is due to the early reduced decomposition of FEC.^[15] Fortunately, this tiny decomposition does not influence the electrochemical window and properties of 3 MF. Figure 1b shows the rate performance of four batteries, 3 MF DIBs exhibit the best performance of those, and delivers the discharge specific of 92.8, 91.6, 90.1, 86.5 and 84.3 mA h/g at 0.5, 0.8, 1.0, 1.5 and 2.0 A/g, respectively. When the current gradually decreased to 0.1 A/g, its capacity recovered to the initial value, indicating an excellent reversibility. As for 3 M DIBs, they only deliver the lower discharge capacity of 64 mA h/g at 2.0 A/g. Not only that, high CE (~100%) of 3 MF is confirmed at high current condition, which is much better than 3 M (~90%) and 0.5 M (~85%). Furthermore, E_{den} is one of the indexes to measure the comprehensive performance of the batteries, and the Ragone plot are presented in Figure S2. Obviously, 3 MF DIBs bring out the highest figure (424.27 Wh/kg at 915.7 W/kg) of those, and comprehensive E_{den} are also excellent under high-power condition (407.77, 399.64, 387.6 and 370.35 Wh/kg at 3598, 4498, 6644 and 8888.4 W/kg, respectively).

Under high-power condition, longer cycling life is helpful for the Na-DIBs to approach the commercial standard. Therefore, we have compared the cycling stability of 3 M and 3 MF at 200–800 mA/g in Figure 2. For detail, Figure 2a shows the various-cycles charge/discharge (CD) curves of two batteries. In fact, there is no obvious difference in performance between two batteries at low current. Figure S3a b shows the first-three CD curves of two batteries at 200 mA/g, which corresponding CV curves are recorded in Figure S3c d. Through the CD curves, the charge/discharge plateaus of two batteries are nondistinctive, and their charge plateaux range include 4.29–4.44 V, 4.44–4.59 V, 4.59–4.74 V and 4.74–4.91 V, which corresponding to GICs at different stages (Stage IV to Stage I).^[16] As for the discharge plateaux, 3 MF shows a special plateau at 4.08 V, which may be caused by FEC. Fortunately, this plateau disappears in the second cycle, and the subsequent CV/CD curves are consistent. Noting that, as the cycles increases, the polarization of 3 M DIBs become more serious, but 3 MF DIBs still keep more stable working condition. And this difference becomes more pronounced at large current density (Figure 2a).

Discharge output voltage is the key parameter to determine energy density, and discharge medium-voltage curves of two batteries are also obtained in Figure 2b. After 500th CD cycles, 3 MF DIBs only lose 0.247 V at 500 mA/g, but 3 M ones lose 0.450 V at same current by 400 CD cycles. As for 800 mA/g, the discharge medium-voltage of 3 M DIBs decrease quickly in the first 50 cycles, which is not comparable to 3 MF DIBs. Clearly, the diving phenomenon causes the performance of 3 M DIB to decline sharply, not only in terms of voltage, but also in terms of capacity and CE (Figure 2c). According to our findings, this phenomenon occurs only under the condition of high-power density, and the batteries usually fails within 100 cycles, which is obviously not conducive to the long-term cycle of the battery.^[17] Nevertheless, 3 MF DIBs exhibit more stable and ideal electrochemical property than 3 M ones. During long cycling process, the CE of 3 MF DIBs always remain stable at 98%, indicating the batteries can store/release electrical energy

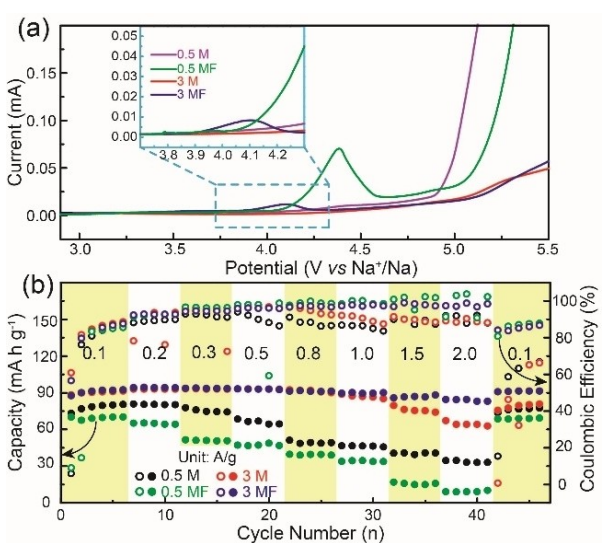


Figure 1. Electrochemical stability and discharge capacity of various electrolytes system. a) the LSV curves of 0.5 M, 0.5 MF, 3 M and 3 MF at 2 mV/s. b) The rate performance and coulombic efficiency of two main electrolytes (3 M and 3 MF), 0.5 M and 0.5 MF at current from 0.1 to 2.0 A/g.

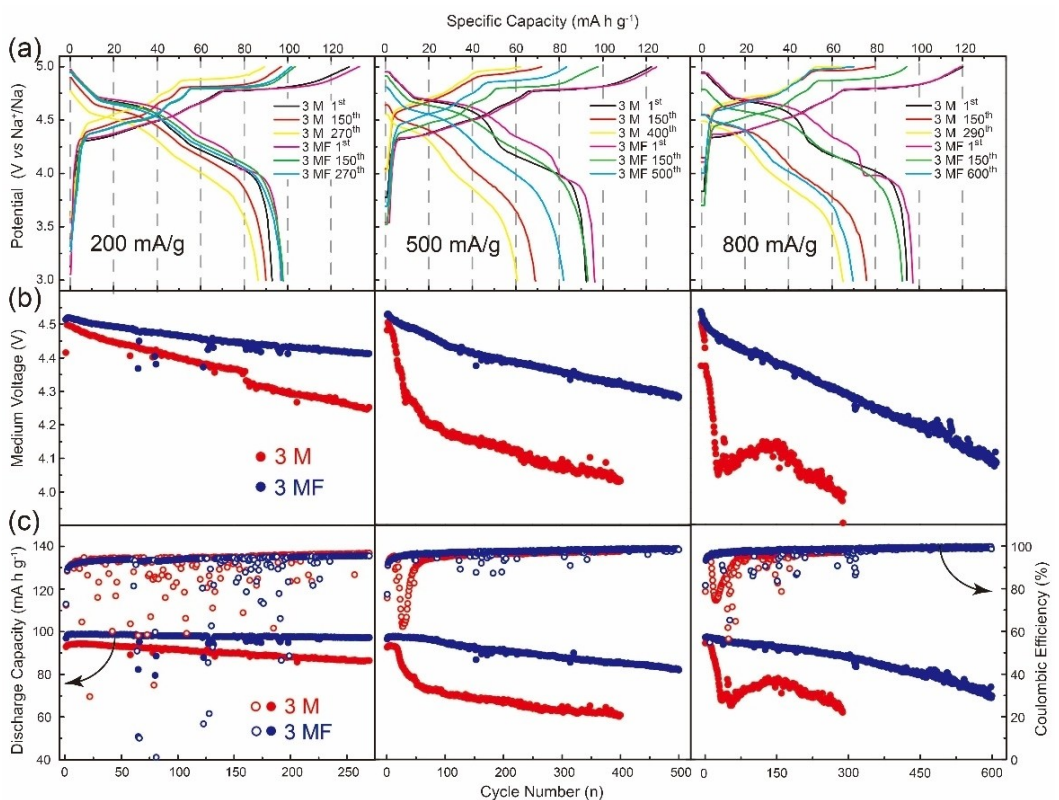


Figure 2. Detailed comparison of electrochemical performance between 3 M and 3 MF DIBs at 200, 500 and 800 mA/g. a) Charge/discharge curves, b) Medium voltage, c) Capacity and coulombic efficiency of two batteries at different cycles under corresponding current densities.

reversibly. Despite the phenomenon of lesser capacity decay, the capacity retention of 500 CD cycles is 89.7% at 500 mA/g (600 CD cycles, 71.6% at 800 mA/g). In a word, 3 MF DIBs show excellent long-cycling ability, which profit from the avoidance of diving phenomenon. To be sure, such DIBs have high- E_{den} stability, although through high-current cycling process, 3 MF DIBs always maintain higher E_{den} (Figure S5), which widens the application prospect of Na-DIBs under high power-density. In addition, the large loading testing of cathode materials is also important for the application of Na-DIBs, and the detailed results and discussions are shown in Figure S6.

As shown in Figure S4a b and Figure 3a, the various scan-rates CV curves and diffusion results of 3 M and 3 MF DIBs were recorded. Although both show the same redox peaks at the corresponding potential (similar voltage plateau in CD curves), 3 MF displays the better property than 3 M under high scan-rates. Firstly, there is a superposition of peak 1 and peak 2 at 0.7 mV/s in Figure S4a, and peak 3 is also superimposed at 1.0 mV/s, which means 3 M DIBs have a serious polarization during rapid-reaction process. Contrary to 3 M DIBs, no peaks superposition was found in 3 MF DIBs at 0.1–1.0 mV/s (Figure S4b). Secondly, with the increase of scan-rates, there is an obvious polarization at high potential reaction (peak 4) in 3 M DIBs, which makes the batteries are difficult to complete the electrochemical process at this time. However, the peaks of 3 MF still remain stable and sharp. Thirdly, 3 MF exhibits higher cathodic peaks than 3 M at all scan-rates, all three cathodic

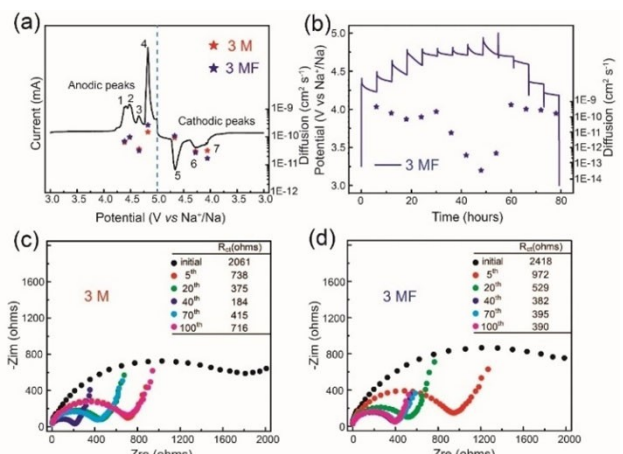


Figure 3. Kinetic analyses of two electrolytes system. a) A complete CV curve of 3 MF, and the diffusion results of two electrolytes. b) The charge/discharge curve of 3 MF, and the diffusion results of each corresponding process. c) EIS analyses of 3 M electrolyte at various cycles. d) EIS analyses result of 3 MF at corresponding cycles.

peaks of 3 MF are higher than 4.0 V. Among them, the potential of peak 5 is as high as 4.7 V, which is consistent with the conclusion in Figure 2b. Furthermore, seven redox peaks of two DIBs were used to measure the dynamic difference, the calculation process and formula were given in the Supporting Information (Figure S7).^[18] The results are presented in Figure 3a, seven dynamics data and a complete CV curve were

labeled at corresponding potentials. On the whole, the dynamics of 3 MF and 3 M is not huge, and both are within the range of $10^{-9} \text{ cm}^2 \text{s}^{-1}$ to $10^{-11} \text{ cm}^2 \text{s}^{-1}$. Noting that, 3 MF shows stronger diffusion ability than 3 M at peak 4 (high charge potential), and weaker than 3 M at peak 7 (low discharge potential). The results of the former are in good agreement with the weaker polarization phenomenon in Figure S4d. As for the result of latter, according to the previous voltage/cycle number curves in Figure 2b, we conjectured that 3 MF electrolyte enhanced the diffusion ability at high potential reaction, conversely, may have some negative impact on low potential. Even so, the high output voltage of the 3 MF DIBs is real and beneficial to the development of high energy storage for Na-DIBs.

In order to further understand the dynamic difference of 3 M DIBs and 3 MF DIBs, Figure 3b shows the galvanostatic CD curve and diffusion analysis of 3 MF DIBs by galvanostatic intermittent titration technique (GITT). The calculation equation is as follows [Equation (1)]:^[19]

$$D_{PF_6^-} = \frac{4}{\pi \tau} \left(\frac{m_B V_M}{M_B S} \right)^2 \left(\frac{\Delta E_s}{\Delta E_r} \right)^2 \left(\tau \ll \frac{L^2}{D} \right) \quad (1)$$

Among them, M_B , V_M and m_B are the molecular weight, molar volume and mass of the active cathode, respectively. Then, τ is the time of each charge or discharge process (300 s), S is the surface area of graphite cathode (1.13 cm^2), L is the average radius of graphite particles. ΔE_s and ΔE_r represents the quasi-equilibrium potential and the change of cell voltage, respectively. After the calculation, most diffusion coefficients of different charge/discharge process are between $10^{-9} \text{ cm}^2 \text{s}^{-1}$ to $10^{-11} \text{ cm}^2 \text{s}^{-1}$, which is consistent with the results of CV curves. However, unlike the CV results, there are several lower diffusion coefficients during the last few charging (4.7–5.0 V) in Figure 4b. The reason for these differences are based by different testing methods, which is common and acceptable. Nonetheless, these weak diffusion processes are worth researching. As

shown in Figure S8, same test conditions were applied to 3 M DIBs. Beyond our expectation, 3 M DIBs cannot accomplish a whole GITT curves, and there are a few serious polarization phenomena at high potential process. For detail, in the local zoom of Figure S7, the voltage increased during each charging is lower than the voltage decreased during the relaxation process. This is due to its weak diffusion ability at high potential, which further indicates that 3 M is inferior to 3 MF in terms of diffusion ability.

To explore the impact of the diving phenomenon for DIBs, the electrochemical impedance spectroscopy (EIS) Nyquist plots of 3 M and 3 MF at various cycles are provided and analyzed in Figure 3c and d, respectively. As shown in Figure S9, the initial charge transfer resistance (R_{ct}) of 3 M and 3 MF is 2061 ohms and 2418 ohms, respectively. Such high initial R_{ct} 's are due to the initial state of the batteries has not been activated.^[19b] After 5 CD cycles, the R_{ct} of both 3 M and 3 MF are reduced to less than 1000 ohms. As the number of cycles increases, the resistance of both shows the downward trend before the 40th cycle, which be due to continuous activation process at high current (500 mA/g). For detail, as shown in the table of Figure 3c and d, the resistances of 3 M and 3 MF show the minimum value of 184 ohms and 382 ohms at 40th cycle, respectively. However, the resistance of 3 M shows an upward trend (415 ohms at 70th, 716 ohms at 100th). To our surprise, the inflection point of the resistance change law occurs in the cycles of the diving phenomenon. After this point, the diffusion ability and electrochemical performance of 3 M DIBs become worse, which is inferior to 3 MF. Furthermore, according to previous researches, the changes of resistance value usually correspond to the change of cathode electrolyte interphase (CEI) film on the electrode surface. Therefore, we speculate the minimum resistance and the subsequent larger resistances correspond to the destruction and random recombination of the 3 M-CEI film, respectively. Undoubtedly, above two behaviors will certainly destroy the cycling stability of the batteries. Interestingly, the 3 MF exhibits stable resistances value after 40th cycle (395 ohms at 70th, 390 ohms at 100th), implying 3 MF-CEI film maintain stable during high-current cycling. Compared with 3 M DIBs, 3 MF DIBs have stabilized in cycling process under high current-densities. Meanwhile, this result is also consistent with the previous conclusions (Figure 2c and Figure S5).

Whether the diving phenomenon occurs is very important to the comprehensive performance (safety, cycling life, capacity and so on) of the Na-DIBs. High-temperature conditions, in which the external environment can provide extra thermal kinetic energy for cells,^[9c,20] were used to explore whether the performance of 3 M DIBs could be improved and avoid diving phenomenon. In Figure 4a, the various-rates discharge curves of 3 M and 3 MF DIBs at 40 °C are represented. 3 M DIBs show the discharge specific capacity of 95, 90, 82, 61 and 40 mAh/g at 0.5, 0.8, 1.0, 1.5 and 2.0 mA/g, respectively, which is not as good as the property of normal temperature environment. What is worse, with the increase of current, the discharge plateau decreases gradually (severe polarization). As for 3 MF DIBs, higher discharge plateau and outstanding rate perform-

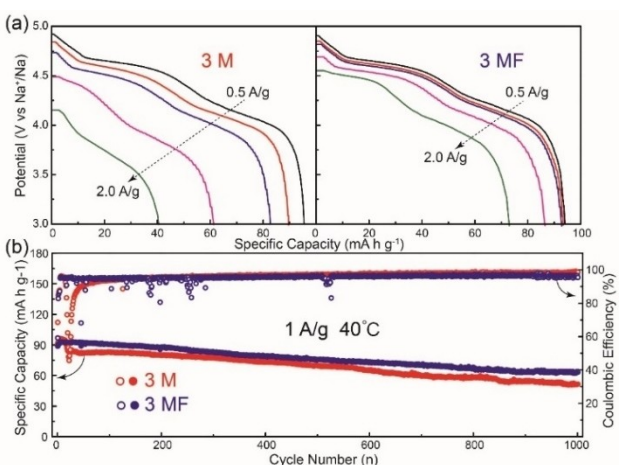


Figure 4. Electrochemical performance of 3 M and 3 MF DIBs at 40°C. a) The discharge curves of 3 M and 3 MF at current from 0.5 to 2.0 A/g. b) c) Long cycling ability of two electrolytes at 1.0 A/g.

ance are still gained (94, 93, 92, 86 and 72 mAh/g at the corresponding current). Herein, the high-temperature long-cycling testing of two batteries at 1.0 A/g is shown in Figure 4b. Not surprisingly, the diving phenomenon still exists in the first 50 cycles of 3 M DIBs, which causes the capacity decay. Furthermore, 3 M DIBs still maintain higher capacity retention of 72% after 1000 cycles. In short, favorable rate performance and cycling stability prove 3 M DIBs have a certain prospect of high temperature application, but the reasons for improving performance and avoiding side reactions have not been explored. In addition, on the basis of EIS results, the interface modification on anode and cathode by two electrolytes should also be discussed.

The 3 MF electrolyte provides obvious protection for graphite cathode in DIBs, mainly for the structural integrity. For example, Figure S10 shows the comparison of XRD patterns between initial graphite electrode, 3 M graphite electrode-100th and 3 MF graphite electrode-100th. And the XRD pattern of graphite powder and the image of (002) crystal surface is shown in Figure S11b. Obviously, as the characteristic peak of graphite, this strong and narrow diffraction peak appears at 26.53° (2θ). It is well known that highly ordered layered structures are important for PF_6^- storage, therefore, the main results of the change at (002) peak as shown in Figure 5a–c. Before the cycling testing, the (002) peak of graphite electrode (Figure 5a) keeps strong and narrow, and consistent with the Figure S11b. But, 3 M graphite electrode shows a weak and broad diffraction peak at 26.38° (2θ) in Figure 5b, which indicates the order of the graphite structure is destroyed and the layer spacing becomes larger after 100th cycles.^[21] However, such a structure is detrimental to the capacity storage for graphite, and further impacts the cycling stability of batteries. As for 3 MF electrode-100th, the XRD pattern of 100th cycles shows acceptable result in Figure 5c. For detail, although the width of the peak increases slightly and the intensity decreases, the diffraction peak keeps at 26.49° (2θ), which is only shifted by 0.04°. Consequently, the protection of 3 MF electrolyte to

graphite electrode is more obvious, mainly reflects in the structural stability, and further guaranteed the cycling stability of batteries.

To further confirm the cathode-protection of 3 MF electrolyte, SEM images of the above three electrodes are shown in Figure 5d–f. Noting that, Figure 5d displays unbroken lamellar structure of initial graphite cathode, which is similar with the initial graphite powder (Figure S11a). However, the structure of 3 M electrode becomes smaller-size and crooked after 100th cycles, the original graphite structure has been destroyed (Figure 5e). In comparison, 3 MF electrode shows higher structural integrity, and the larger graphite sheets are clear in Figure 5f. The results of SEM images are consistent with XRD patterns. Based on the above conclusion, it can be confirmed that 3 MF electrolyte can alleviate the destruction of the structure of graphite during cycling, which may be closely related to the excellent CEI film. Hence, the EDX element content of three electrodes is evaluated in Figure S12. In Figure S12a, carbon is present in all three: graphite, conductive carbon black and PVDF; Oxygen comes from the hydroxyl and carbonyl in conductive carbon black; Fluorine comes mainly from PVDF. As shown in Figure S12b, due to the formation of CEI film and the decomposition of NaPF_6 , the content of oxygen and fluorine are both higher than initial graphite electrode by 3 M electrolyte.^[22] Similarly, sodium and phosphorus both come from NaPF_6 . In contrast to 3 M, 3 MF electrolyte increases the content of F, Na and P on electrode surface (Figure S12c). In other words, 3 MF electrolyte promotes the electrochemical decomposition of salt to form the CEI film with rich-inorganic components on the electrode surface, which can effectively alleviate the expansion/contraction of graphite and maintain the structural integrity during intercalation and de-intercalation.

The XPS analysis is used to understand the composition of the electrode surface, and Figure 5g–i shows the reaction changes of C 1s spectra for graphite electrode surface. In Figure 5g, the peak of C–C bond at 283.58 eV is the characteristic peak of graphite, the peaks of C–O (284.98 eV) and C–F (298.98 eV) represent the carbon black and PVDF,^[1b] such a large difference in peaks strength is consistent with graphite as the main composition of the electrode. After electrochemical testing with 3 M electrolyte, the peak of C–O bond increases in C 1s spectra (Figure 5h), which means only a little organic component exist on CEI film surface. Although the emergence of ROCO_2Na (286.88 eV) explains the decomposition of NaPF_6 on graphite cathode, this peak is much weaker than 3 MF one (Figure 5i). The stronger peak of ROCO_2Na represents higher decomposition content of sodium salt, not only that, this CEI film can be maintained stably during long cycling process. Furthermore, the increase of C–O peak and the appearance of C–OH (286.58 eV) and C–O–C (285.58 eV), explaining the 3 MF CEI film has certain content organic component. At the same time, inorganic component in CEI film also can ensure the structure stability of graphite cathode during charging/discharging, the F 1s and P 2p spectra of 3 M and 3 MF is shown in Figure S12. The strength of the $\text{Na}_x\text{PO}_y\text{F}_z$ peak (685.08 eV) is difficult to be compared because of the high strength of the

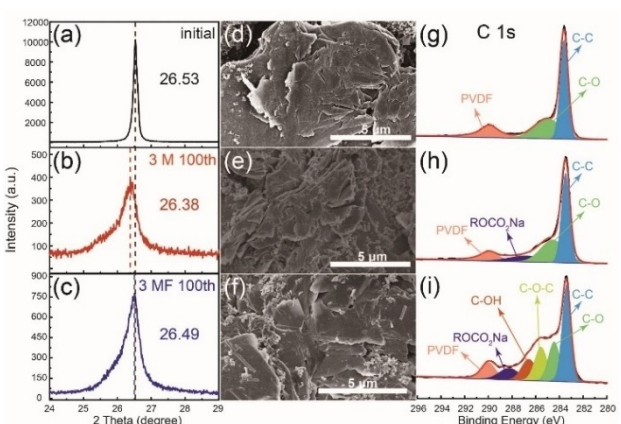


Figure 5. Physical characterization of initial graphite electrode, 3 M graphite electrode-100th and 3 MF graphite electrode-100th. a, b and c) Local XRD patterns of above three electrodes at 2θ from 24 to 29°. d, e and f) SEM images of above three electrodes. g, h and i) XPS analyses of above three electrodes.

P–F bond, but this can still indicate that the inorganic component is formed on the graphite cathode surface.^[8b] Noting that, the P 2p spectra of two electrodes shows the significant differences. There are no obvious peaks of P 2p in Figure S12c, but three P 2p peaks are recorded in 3 MF CEI film (Figure S13d), which including P–F (135.88 eV), Na_xPO_yF_z (133.68 eV) and P–C (or P–O–C 132.58 eV).^[8b,23] According to the above findings, the 3 M CEI film with less organic and inorganic component cannot effectively protect graphite cathode, which may be the cause of diving phenomenon. Fortunately, 3 MF electrolyte can form a better CEI film with higher-content organic and inorganic component, and this CEI film is stable during long-term cycling, which guarantees the outstanding performance of the 3 MF DIBs.

In addition, the protection of this novel electrolyte for sodium metal anode is also worth researching. However, considering that the practical application of Na-DIBs requires sodium-free anode, so we have less research on sodium metal anode. The galvanostatic deposition/stripping voltage profiles of two electrolytes for symmetric cells (SC) are shown in Figure S14. Under the current density of 1 mA/cm², 3 MF SC shows a larger overpotential (326 mV) than 3 M (189 mV) in the first cycle, which is due to the formation of solid electrolyte interphase (SEI) film by the decomposition of the FEC.^[24] However, the overpotential of 3 MF SC decreases and stabilizes at 176 mV, but 3 M SC shows the terrible performance, whose overpotential reached more than 1 V after 29 hours cycles. Clearly 3 M electrolyte cannot preserve the stability of the metal anode in fast deposition/stripping process (10 mins for each process). Interestingly, 3 MF exhibits outstanding overpotential of 240 mV after 60 hours cycles, which means 3 MF electrolyte has an obvious protective effect on sodium anode, and is conducive to extending the cycling life of Na-based DIBs.

Figure 6 shows our modified strategy for DIBs, conventional electrolyte gives the poor performance for DIBs: low CE and low energy density. Increasing the electrolyte concentration,

although the energy density and initial CE both are improved, serious diving phenomenon has inhibited the cycling stability and practicability of Na-DIBs. Fortunately, this novel 3 MF electrolyte makes a great breakthrough in the performance of DIBs, which achieve high energy density, long-cycling ability and high CE (low safety hazard). This is attributed to the simultaneous modification of 3 MF to the anode and cathode interfaces, which reduces the overpotential in the cycling process, and ensures the structural stability of the graphite cathode by a larger number of free anions and FEC solvent.^[11a,12a,25] It is important to note that these modified-electrolyte DIBs have certain application significance, which could light up many LED lights (3 V).

3. Conclusions

In summary, we have successfully enhanced the comprehensive performance of Na-DIBs at high power density by novel 3 MF electrolyte, this electrolyte not only avoid the diving phenomenon, but also improve the E_{den} of Na-DIBs and promote the long-cycling stability under high-power condition, which is due to its protection for sodium-anode and graphite-cathode. Furthermore, under high potential reaction during charging, the optimization of diffusion process similarly achieves the excellent performance. Considering the cost of the battery design, our modification technique is simple and inexpensive. This research set directions for the modification design of DIBs electrolytes, and further promote the applied possibilities of Na-DIBs.

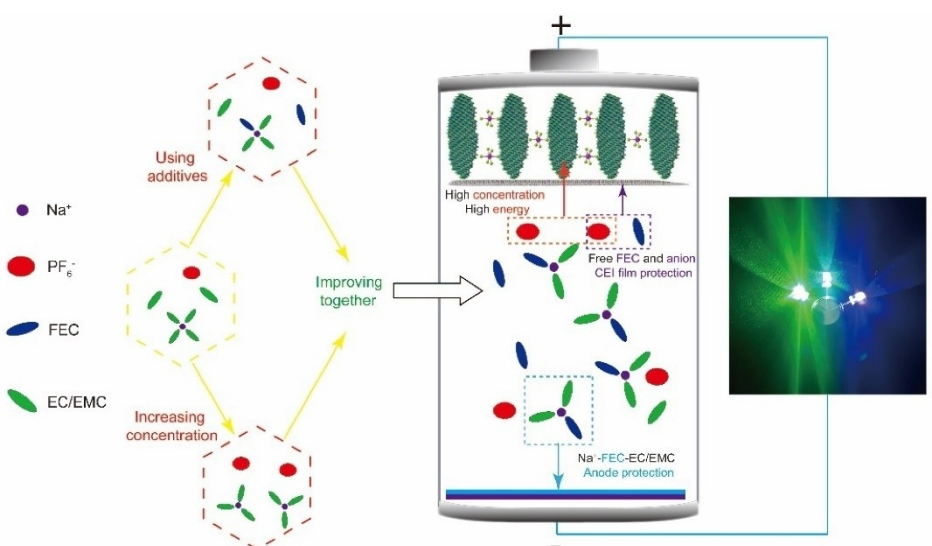


Figure 6. The scheme illustration displaying the modified strategy for Na-DIB.

Acknowledgements

This work was financially supported by the National Natural Science Foundation of China (No. 91963118), and the 111 Project (No. B13013).

Conflict of Interest

The authors declare no conflict of interest.

Keywords: cathode protection · cycling stability · diving phenomenon · dual-ion batteries · energy density

- [1] a) Y. Sui, C. Liu, R. C. Masse, Z. G. Neale, M. Atif, M. AlSalhi, G. Cao, *Energy Storage Mater.* **2020**, *25*, 1; b) W. H. Li, Q. L. Ning, X. T. Xi, B. H. Hou, J. Z. Guo, Y. Yang, B. Chen, X. L. Wu, *Adv. Mater.* **2019**, *31*, 1804766; c) R. T. Carlin, C. Hugh, J. Fuller, P. C. Trulove, *J. Electrochem. Soc.* **1994**, *141*, L73.
- [2] a) C. Zhao, Y. Lu, L. Chen, Y. S. Hu, *InfoMat* **2020**, *2*, 126; b) Z.-Y. Gu, J.-Z. Guo, X.-X. Zhao, X.-T. Wang, D. Xie, Z.-H. Sun, C.-D. Zhao, H.-J. Liang, W.-H. Li, X.-L. Wu, *InfoMat* **2021**, *3*, 694..
- [3] a) X. Zhou, Q. Liu, C. Jiang, B. Ji, X. Ji, Y. Tang, H. M. Cheng, *Angew. Chem. Int. Ed.* **2020**, *59*, 3802; b) T. Placke, A. Heckmann, R. Schmuck, P. Meister, K. Beltrop, M. Winter, *Joule* **2018**, *2*, 2528; c) M. Wang, Y. Tang, *Adv. Energy Mater.* **2018**, *8*, 1703320; d) P. Meister, O. Fromm, S. Rothermel, J. Kasnatscheew, M. Winter, T. Placke, *Electrochim. Acta* **2017**, *228*, 18; e) X. Qi, B. Blizanac, A. DuPasquier, P. Meister, T. Placke, M. Oljaca, J. Li, M. Winter, *Phys. Chem. Chem. Phys.* **2014**, *16*, 25306.
- [4] M. Zhang, X. Song, X. Ou, Y. Tang, *Energy Storage Mater.* **2019**, *16*, 65.
- [5] a) M. Acerce, D. Voiry, M. Chhowalla, *Nat. Nanotechnol.* **2015**, *10*, 313; b) Z. Yu, L. Tetard, L. Zhai, J. Thomas, *Energy Environ. Sci.* **2015**, *8*, 702; c) R. Wang, M. Yao, Z. Niu, *InfoMat* **2020**, *2*, 113.
- [6] a) X. Zhao, S. Ren, M. Bruns, M. Fichtner, *J. Power Sources* **2014**, *245*, 706; b) F. Gschwind, G. Rodriguez-Garcia, D. J. S. Sandbeck, A. Gross, M. Weil, M. Fichtner, N. Hörmann, *J. Fluorine Chem.* **2016**, *182*, 76; c) F. Chen, Z. Y. Leong, H. Y. Yang, *Energy Storage Mater.* **2017**, *7*, 189.
- [7] L. Fan, Q. Liu, S. Chen, Z. Xu, B. Lu, *Adv. Energy Mater.* **2017**, *7*, 1602778.
- [8] a) J. A. Read, A. V. Cresce, M. H. Ervin, K. Xu, *Energy Environ. Sci.* **2014**, *7*, 617; b) X. Xu, K. Lin, D. Zhou, Q. Liu, X. Qin, S. Wang, S. He, F. Kang, B. Li, G. Wang, *Chem* **2020**, *6*, 902; c) Z. Hu, Q. Liu, K. Zhang, L. Zhou, L. Li, M. Chen, Z. Tao, Y. M. Kang, L. Mai, S. L. Chou, J. Chen, S. X. Dou, *ACS Appl. Mater. Interfaces* **2018**, *10*, 35978.
- [9] a) M. D. Slater, D. Kim, E. Lee, C. S. Johnson, *Adv. Funct. Mater.* **2013**, *23*, 947; b) N. Yabuuchi, K. Kubota, M. Dahbi, S. Komaba, *Chem. Rev.* **2014**, *114*, 11636; c) C. Yang, S. Xin, L. Mai, Y. You, *Adv. Energy Mater.* **2020**, DOI: 10.1002/aenm.202000974; d) M. Yang, Q. Ning, C. Fan, X. Wu, *Chin. Chem. Lett.* **2020**, *32*, 895; e) B. H. Hou, Y. Y. Wang, Q. L. Ning, W. H. Li, X. T. Xi, X. Yang, H. J. Liang, X. Feng, X. L. Wu, *Adv. Mater.* **2019**, *31*, 1903125.
- [10] a) C. Y. Chen, K. Matsumoto, K. Kubota, R. Hagiwara, Q. Xu, *Adv. Funct. Mater.* **2020**, *30*, 2003557; b) Y. Wang, Y. Zhang, Q. Duan, P.-K. Lee, S. Wang, D. Y. W. Yu, *J. Power Sources* **2020**, *471*, 228466; c) R. Nozu, E. Suzuki, O. Kimura, N. Onagi, T. Ishihara, *Electrochim. Acta* **2020**, *337*, 135711.
- [11] a) L. Xiang, X. Ou, X. Wang, Z. Zhou, X. Li, Y. Tang, *Angew. Chem. Int. Ed.* **2020**, *59*, 17924; b) M. Balabajew, T. Kranz, B. Roling, *ChemElectroChem* **2015**, *2*, 1991; c) K. Beltrop, X. Qi, T. Hering, S. Röser, M. Winter, T. Placke, *J. Power Sources* **2018**, *373*, 193; d) A. Heckmann, J. Thienenkamp, K. Beltrop, M. Winter, G. Brunklaus, T. Placke, *Electrochim. Acta* **2018**, *260*, 514; e) S. Wang, X. Xiao, C. Fu, J. Tu, Y. Tan, S. Jiao, *J. Mater. Chem. A* **2018**, *6*, 4313; f) W.-H. Li, H.-J. Liang, X.-K. Hou, Z.-Y. Gu, X.-X. Zhao, J.-Z. Guo, X. Yang, X.-L. Wu, *J. Energy Chem.* **2020**, *50*, 416.
- [12] a) X. Jiang, X. Liu, Z. Zeng, L. Xiao, X. Ai, H. Yang, Y. Cao, *Adv. Energy Mater.* **2018**, *8*, 1802176; b) D. Xie, M. Zhang, Y. Wu, L. Xiang, Y. Tang, *Adv. Funct. Mater.* **2019**, *30*, 1906770.
- [13] S. Aladinli, F. Bordet, K. Ahlbrecht, J. Tübke, M. Holzapfel, *Electrochim. Acta* **2017**, *231*, 468.
- [14] X. Li, X. Ou, Y. Tang, *Adv. Energy Mater.* **2020**, *10*, 2002567.
- [15] Z. Wang, H. Yang, Y. Liu, Y. Bai, G. Chen, Y. Li, X. Wang, H. Xu, C. Wu, J. Lu, *Small* **2020**, *16*, 2003268.
- [16] J. A. Read, *J. Phys. Chem. C* **2015**, *119*, 8438.
- [17] J. Xu, R. D. Deshpande, J. Pan, Y.-T. Cheng, V. S. Battaglia, *J. Electrochem. Soc.* **2015**, *162*, A2026.
- [18] a) X. Wang, L. Qi, H. Wang, *ACS Appl. Mater. Interfaces* **2019**, *11*, 30453; b) B. Wang, Y. Cheng, H. Su, M. Cheng, Y. Li, H. Geng, Z. Dai, *ChemSusChem* **2020**, *13*, 4078.
- [19] a) M. Y. Wang, J. Z. Guo, Z. W. Wang, Z. Y. Gu, X. J. Nie, X. Yang, X. L. Wu, *Small* **2020**, *16*, 1907645; b) S. Miyoshi, T. Akbay, T. Kurihara, T. Fukuda, A. T. Staykov, S. Ida, T. Ishihara, *J. Phys. Chem. C* **2016**, *120*, 22887.
- [20] X. X. Zhao, Z. Y. Gu, W. H. Li, X. Yang, J. Z. Guo, X. L. Wu, *Chem. Eur. J.* **2020**, *26*, 7823.
- [21] a) K. Kim, Q. Guo, L. Tang, L. Zhu, C. Pan, C. Chang, J. Razink, M. Lerner, C. Fang, X. Ji, *Angew. Chem. Int. Ed.* **2020**, *59*, 1; b) H.-J. Liang, B.-H. Hou, W.-H. Li, Q.-L. Ning, X. Yang, Z.-Y. Gu, X.-J. Nie, G. Wang, X.-L. Wu, *Energy Environ. Sci.* **2019**, *12*, 3575.
- [22] N. von Aspern, D. Diddens, T. Kobayashi, M. Borner, O. Stubbmann-Kazakova, V. Kozel, G. V. Rosenthaler, J. Smiatek, M. Winter, I. Cekic-Laskovic, *ACS Appl. Mater. Interfaces* **2019**, *11*, 16605.
- [23] X. Wang, S. Wang, K. Shen, S. He, X. Hou, F. Chen, *J. Mater. Chem. A* **2020**, *8*, 4007.
- [24] a) L. Yu, Q. Su, B. Li, W. Liu, M. Zhang, S. Ding, G. Du, B. Xu, *Electrochim. Acta* **2020**, *362*, 137130; b) J. Luo, M. Edward, H. Wang, X. Tao, W. Li, *InfoMat* **2020**, *2*, 1057.
- [25] J. Ming, Z. Cao, Q. Li, W. Wahyudi, W. Wang, L. Cavallo, K.-J. Park, Y.-K. Sun, H. N. Alshareef, *ACS Energy Lett.* **2019**, *4*, 1584.

Manuscript received: May 31, 2021

Accepted manuscript online: June 11, 2021

Version of record online: July 1, 2021